Available online at www.sciencedirect.com
ScienceDirect
Journal of Molecular Catalysis A: Chemical 282 (2008) 9–21
JOURNAL OF MOLECULAR CATALYSIS A: CHEMICAL
www.elsevier.com/locate/molcata

Editors Choice Paper

Effect of hydrogen sulfide on the catalytic activity of Ni-YSZ cermets

John N. Kuhn, Nandita Lakshminarayanan, Umit S. Ozkan *

The Ohio State University, Department of Chemical and Biomolecular Engineering, Columbus, OH 43210, USA

Available online 5 December 2007

Abstract

Ability to operate solid oxide fuel cells (SOFCs) on fuels containing carbon and sulfur with a minimal amount of deactivation is an important technical hurdle. For this reason, the influence of H_2S upon the activity and stability of Ni-YSZ (yttria-stabilized zirconia) cermets was examined for model anode chamber reactions. Reactions with H_2O (water-gas shift reaction, steam reforming) were more strongly affected by sulfur compared to CO or CH_4 oxidation reactions. For reactions involving CH_4, hydrocarbon decomposition was the dominant reaction pathway at higher temperatures; however, this reaction path was inhibited by sulfur exposure. Changes in the steam reforming activity of sulfur-treated samples with increasing temperature or with high-temperature H_2 treatment suggested sulfur migration to more active sites or surface restructuring. Such changes in active sites appear to be accelerated in the presence of H_2O. Direct poisoning of YSZ was eliminated since activity differences for the water-gas shift reaction, CH_4–H_2O reforming, and partial CH_4 oxidation were negligible with and without H_2S exposure. Reaction results were complemented by X-ray diffraction (XRD), laser Raman spectroscopy (LRS), X-ray photoelectron spectroscopy (XPS), and diffuse reflectance infrared Fourier transform spectroscopy (DRIFTS) with CO as a probe molecule.

Keywords: SOFC; Ni-YSZ; Catalyst deactivation; Sulfur; Carbon deposition

1. Introduction

Solid oxide fuel cells (SOFCs) are expected to be a crucial technology in the future of power generation [1,2]. SOFCs offer many desirable advantages compared to other types of fuel cells and conversion devices due to their high efficiency, low pollution, lack of moving parts, ability to circumvent precious metal use, use of solid electrolytes, and fuel flexibility. However, commercialization is currently impeded by high costs and deactivation, which limit lifetime and performance. While some issues (e.g., high operating temperature and stability) arise due to cathode electrocatalyst concerns, technological challenges also exist for anode electrocatalysts. These problems occur when fuel is no longer high purity H_2. Since SOFCs are envisioned to generate power from carbonaceous fuels containing S (syngas derived from coal or biomass, natural gas, etc.) and not pure H_2, a major challenge is developing effective and economic materials and conditions in the anode chamber that do not lead to deactivation caused by S and C interactions with the surface of the electrocatalysts.

The range of possible anode electrocatalysts is limited by the selection criteria, which demand that the materials be electronic and ionic conductors, compatible with other SOFC components (e.g., non-reactive and similar in thermal properties), and catalytically active for electrochemical oxidation and fuel processing reactions (e.g., the water-gas shift reaction, reforming). After considering these requirements, several alternatives to the conventional Ni-yttria stabilized zirconia (YSZ) cermet anodes exist for use with S-containing fuels such as S-containing materials, mixed conductors, and non-Ni-based or alloyed cermets. S-containing materials such as $CuFe_2S_4$, $NiFe_2S_4$, WS_2, $CuCo_2S_4$, and CoS_2 were tested in SOFCs with H_2S as the fuel, but deactivation occurred during long-term studies [3]. Co-Mo-S showed stable performance for 5 days with H_2S as the fuel, but required Ag to improve conductivity [4] and the introduction of CO led to performance losses [5] so use with C-containing fuels is limited. The study of mixed conductors, primarily based on perovskite-type (ABO_3) or related structures, is a rapidly developing field [6,7]. Promising anode candidate materials include those with Mn [8], V [9,10], Ti [11–13], Cr and

* Corresponding author. Tel.: +1 614 292 6623; fax: +1 614 292 3769.
E-mail address: Ozkan.1@osu.edu (U.S. Ozkan).

1381-1169/$ – see front matter © 2007 Elsevier B.V. All rights reserved.
doi:10.1016/j.molcata.2007.11.032

V [14,15], Cr and Mn [16,17], or Mg and Mo [18,19] occupying the transition metal site. Although these materials generally showed better fuel flexibility through reduced coke formation (or ability to operate at lower H_2O to C ratios), better stability under redox cycling, and improved S tolerance (when tested) compared to Ni-YSZ, no alternatives currently display enough promise to currently justify its use. Mainly, these materials are unable to conduct electrons rapidly enough when materials were in the form of porous electrodes or when H_2O was present [20–23].

In addition to traditional Ni-YSZ cermets, much energy has gone into developing Cu-ceria anode materials [23,24]. Although these materials demonstrate improved tolerance towards coke deposits [25–27] and S [28,29] compared to Ni-YSZ anodes, Cu-ceria materials are limited by poor thermal stability due to Cu sintering and low power densities/fuel conversions compared to ceramics [18,19] and Ni-YSZ, especially in H_2-rich streams since both Cu and ceria are poor H_2 oxidation catalysts [3]. High-temperature stability was enhanced by the addition of Cr, but the oxidation of Cr by H_2O was then problematic [30]. In addition to replacing Ni with Cu or other metals [31], alloying other transition metals with Ni showed promise [27,32,33]. However, despite their limitations in terms of S and C deactivation, Ni-YSZ anodes presently remain the material of choice due to a lack of proven alternatives.

Since Ni-YSZ is still the material of choice, it is desirable to understand the mechanism of S and C deactivation since such information is applicable to mitigating deactivation and to developing S and coke tolerant and stable alloy formulations. Due to the use of metallic Ni to grow fibers, the phenomenon of coke formation is better understood. After C species adsorb onto the metallic Ni surface and then migrate into it, fibers grow out of the surface [23,34–36]. The phenomenon is kinetically driven as the rate of adsorption to Ni occurs much more rapidly than oxidation by electrochemical oxygen spillover or by H_2O [23,35–38]. Despite the tendency to form coke, Ni-YSZ electrocatalysts showed the ability to directly use CH_4/natural gas (e.g., [39,40]) although there is debate to whether it is practical [23]. Also as cathode improvements (i.e., ability to operate at lower temperatures) are made, C-surface interactions may change as the thermodynamics for methanation and the Boudouard reaction change.

Similar to coke formation, thermodynamic predictions of stable operation regimes are not accurate [41] and the nature of the S-surface interactions may change as the operating temperature becomes lower [41–43]. Introduction of H_2S, even at levels as low as 2 ppm at 1000 °C and 0.2 ppm at 700–900 °C [41–43] and also higher concentrations [44,45] (for Ni-doped ceria anodes), to the anode chamber led to performance losses. At high concentrations (>100 ppm), performance losses were caused by the formation of bulk Ni–S species [3,44–46]. Although the H_2S degradation mechanism at low concentrations (<100 ppm) is not as well understood, experimental and theoretical studies suggest the formation of chemisorbed S on Ni (which are unstable when H_2S is removed from the feed) as the source of deactivation [3,29,41–43]. Deactivation on multiple time scales was also recently observed with the rapid and initial stage being attributed to dissociative chemisorption of H_2S on Ni [43]. A secondary effect was observed at longer times and is speculated to be caused by Ni surface reconstruction or S-electrolyte interactions. YSZ was implicated in the deactivation mechanism because it demonstrated greater susceptibility to H_2S than Sc-stabilized zirconia (SSZ) [41]. Reconstruction of surface Ni by S is supported by other studies which show that relevant reactions are structure sensitive over Ni (e.g., [36,47]). S-induced increase in Ni surface density is believed to be a general phenomenon at elevated temperature and high S-surface coverage [36]. Since steps are more active than terraces for CH_4 activation [48,49], an increase in Ni surface density would cause a loss in activity.

In addition to these direct deactivation processes, synergistic processes can also occur. Both S and C preferentially cover the more active step sites leaving only the less active terrace sites available for catalysis [48,49]. Moreover, the blockage of Ni sites by adsorbed S led to less C deposition [34–36,38,48–52]. The phenomenon arises either because a larger ensemble of Ni sites is needed for graphitization compared to gasification or a larger activity difference exists between these two pathways over the terrace sites compared to the step sites. Additionally, increasing the amount of H_2O to reduce C deposition can lead to accelerated deactivation by making it easier for S to find Ni sites [53].

The present work examined the influence of H_2S upon the activity for selected reactions that are present in an anode compartment of a SOFC operating on syngas. The focus is on establishing a relationship between activity and S-induced changes in the catalyst. In addition to adding clarity to potential deactivation mechanisms, the present work simultaneously evaluates the synergistic relation between the presence of S (and S-induced changes) and coke formation. Moreover, the role of YSZ in reaction and S deactivation processes was evaluated. To better correlate reaction results with the exposure conditions, any polarization effects (which are important for H_2S oxidation rates but not for H_2S deactivation rates [43]) that would influence the intrinsic activity or surface chemistry changes are assumed negligible.

2. Experimental

2.1. Catalyst details

NiO-YSZ (yttria-stabilized zirconia) was supplied by NexTech Materials. The as-received sample was, on a mass basis, 60% NiO and 40% YSZ. The YSZ portion of the sample was 92% zirconia and 8% yttria on a molar basis. For comparison purposes, YSZ (same composition) and Ni_3S_2 (both from Sigma–Aldrich) were also characterized as needed.

Static surface area and pore volume measurements were made by the physical adsorption–desorption of N_2 (or Kr when noted) at 77 K on an ASAP 2010 (Micromeritics). Surface area (SA) was determined by fitting data with the BET isotherm. Total pore volume was based on desorption of pores between 17 and 3000 Å. For YSZ, the BET SA and the pore volume were 114 m^2/g and 0.40 cm^3/g, respectively. For NiO-YSZ, the BET SA and the pore volume were 2.7 m^2/g and 0.02 cm^3/g, respec-

tively. BET SA was repeated accurately (2.5 m^2/g) with Kr as the probe molecule.

2.2. Reaction testing

Reaction experiments were performed with an Autochem II 2920 (Micromeritics) at atmospheric pressure (0.97 atm). As in all experiments, gases were from Praxair in the highest available purity with further in-stream gas clean-up performed. Samples (100 mg post-reduction to Ni, except YSZ which was done on an equal oxide mass) were loaded into U-tube reactors. Prior to the reaction, NiO-YSZ was reduced in 10% H_2/inert at 700 °C for 1 h plus an optional and variable exposure to H_2S (more details provided in Section 2.3). The reactor effluent was analyzed by a Cirrus RGA-MS (MKS instruments). This instrument was used in selected ion mode with the electron multiplier detector. Signals were converted into concentrations using the ionization probability and fragmentation patterns for all species present.

Unless otherwise noted, the reaction involved a temperature ramp at 10 °C/min from 50 to 700 °C where it was held isothermally for 4 h. Reactant flows were as follows for the various reactions: carbon monoxide oxidation (50.0 mL (STP)/min of 6.7% CO/3.3% O_2/He), water-gas shift (52.5 mL (STP)/min of 4.8% CO/4.8% H_2O/He), reverse water-gas shift (50.0 mL (STP)/min of 5.0% CO_2/5.0% H_2/He), methane-steam reforming (52.5 mL (STP)/min of 4.8% CH_4/4.8% H_2O/He), and methane partial oxidation (50.0 mL (STP)/min of 5.0% CH_4/5.0% O_2/He). Steam was supplied using the Autochem's vaporizer that was maintained at the appropriate temperature using Antoine's equation. Following selected reactions, samples were cooled at 10 °C/min under He (30 mL/min) to 50 °C and a temperature-programmed oxidation (TPO) was performed (same MS acquisition parameters as the reaction) using 50 mL/min of 10% O_2/He. Samples were heated at 10 °C/min to 850 °C where it was held isothermally for 20 min. Quantitative reaction parameters were defined as follows:

Onset temperature = $T_{onset\text{-}X}$ = Temperature at which consumption of reactant X or formation of product X begins.
Light-off temperature = $T_{50\text{-}X}$ = Temperature at which conversion of reactant X is 50%.
% Reactant conversion = C_X = 100% × (moles of X converted)/(moles of X in feed).
% Product yield when A is H_2 or H_2O = Y_A = 100% × (2 × moles of A produced)/(total moles of H in the feed).
% Product yield when B is CO or CO_2 = Y_B = 100% × (moles of B produced)/(moles of C in the feed).

Carbon deposition (C_{dep}) was calculated by integrating the CO_2 signal (m/z = 44 after correcting the signal as discussed above) during the TPO after the quenching in He following the steady reaction at 700 °C for 4 h. Data reduction was performed with the Grams AI software package. Integrated areas were multiplied by the total flow rate to calculate the volume of CO_2 formed, which was then converted into a mass of carbon (mg C) deposited using the ideal gas equation and other appropriate factors. Finally, this value was divided by the surface area of the catalyst (0.25 m^2) and the time (4 h) held at 700 °C to arrive at the units of mg C/m^2/h. In addition to the value just described for the average coke deposition rate, a second parameter was calculated as follows for carbon deposition selectivity.

$$\%\ \text{deposited carbon selectivity} = S_C = 100\% \times \frac{\text{moles of C deposited per time}}{\text{moles of } CH_4 \text{ converted per time}}$$

2.3. Catalyst characterization

NiO-YSZ samples were treated *ex situ* (the *in situ* reduction monitored by XRD is the lone exception). Treatments were performed by placing the NiO-YSZ sample in a quartz reactor placed in a furnace and Brooks mass flow controllers were used to expose the sample to desired concentrations. Appropriate gas regulators and mass flow controllers were employed for safely handling H_2S. Samples were treated by reducing 10% H_2/inert (50 mL/min) at 700 °C for 1 h plus an optional and variable exposure to H_2S (50–500 ppm at 20 mL/min) with a N_2 balance. While heating (10 °C/min) occurred under the reducing gas, all samples were cooled (same rate) under pure N_2. A summary of the H_2S treatments, as well as all reference compounds studied, is provided in Table 1.

X-ray power diffraction (XRD) patterns were acquired with a Bruker D8 Advance diffractometer equipped with an HTK 1200

Table 1
Notation for treatments of NiO-YSZ catalysts

Notation	Source/treatment
YSZ	As-received from Sigma–Aldrich
NiO-YSZ	As-received from NexTech Materials
Ni-YSZ	Reduced in 10% H_2/inert at 700 °C for 1 h (all samples reduced in this manner first and simplified as just reduced)
Ni-YSZ-50	Reduced and then exposed to 50 ppm H_2S/N_2 for 5 h at 700 °C
Ni-YSZ-50/red	Reduced, then exposed to 50 ppm H_2S/N_2 for 5 h at 700 °C, and then reduced again in 10% H_2/N_2 at 700 °C for 5 h
Ni-YSZ-50/24	Reduced and then exposed to 50 ppm H_2S/N_2 for 24 h at 700 °C
Ni-YSZ-100	Reduced and then exposed to 100 ppm H_2S/N_2 for 5 h at 700 °C
Ni-YSZ-500	Reduced and then exposed to 500 ppm H_2S/N_2 for 5 h at 700 °C
Ni_3S_2	As-received from Sigma–Aldrich

sample holder with controlled temperature and atmosphere capabilities. The instrument was furnished with a Cu $K\alpha_1$ radiation source, an incident beam Ge (1 1 1) monochromator, incident beam Soller slits, and a Braun position sensitive detector (8°). The current and the voltage were 50 mA and 40 kV, respectively. Room temperature measurements were obtained with a 9-sample holder (rotating polyethylene holders with a 0.5 mm deep reservoir) for 2θ values from 20 to 90° at a step size of 0.0144° and a dwell time of 1 s. Other experimental parameters were as follows: 1° divergence slit, 0.5° anti-scatter slit, and 0.75 in. detector width.

In situ XRD analyses were made with the HTK 1200 oven equipped with graphite windows. Acquisition details were the same as above except no rotation was used and the step size was 0.0360°. Samples were loaded onto an alumina holder. A heating rate of 10 °C/min and a 10 min hold time before scanning at each temperature were also employed. The flow rate of the gas, 5% H_2/N_2, was 10 mL/min.

Raman spectra were acquired with Horiba-Jobin Yvon LabRam HR Raman Microscope equipped with an internal He-Ne red laser (633 nm) and an 800 mm focal length spectrometer. Spectra were obtained with a power of 5 mW at the sample, the 1800 grating, and 50× long working distance objective. Acquisition number and time were altered depending on the sample's scattering ability.

X-ray photoelectron spectroscopy (XPS) data were attained with a Kratos Ultra Axis Spectrometer using Al Kα radiation (operated at 13 kV and 10 mA) under vacuum ($<2 \times 10^{-9}$ Torr). Samples were ground into carbon tape for analysis. With a slot aperture setting, the spectrometer was used in spectrum analyzer and hybrid lens mode. The charge neutralizer was set at a current of 2.1 A, a bias of 1.3 V, and a charge of 2.2 V during analysis. The C1s peak at 284.5 eV was used for binding energy correction. A survey scan (1 sweep/100 ms dwell) was acquired between 1400 and 0 eV. Concurrent region sweeps for Ni2p (4/400), O1s (4/75), C1s (4/150), and a combined section Y3d, Zr3d, and S2p (4/600) were obtained. Deconvolution was performed with Gaussian curves using XPS Peak 4.1 program. Elemental surface composition was calculated using transmission values and relative sensitivity factors specific for the instrument equipped with an Al source.

In situ DRIFT spectra were acquired with a Thermoelectron Nicolet 6700 FTIR spectrometer furnished with a MCT detector and an environmental chamber. Spectra were obtained at a resolution of 4 cm^{-1} using 500 scans between 650 and 4000 cm^{-1}. Once in the environmental chamber, samples were treated in He (30 mL/min) at 550 °C for 30 min. A separate experiment was performed with a MS to confirm that sulfur species did not desorb below this temperature. Upon cooling, backgrounds were collected in the same flow following 5 min holds after the temperature was lowered. At 50 °C, samples were exposed to 2% CO/Ar (30 mL/min) for 30 min. Then, the chamber was purged for 15 min. The temperature was raised in 50 °C increments after which the temperature was held constant for 5 min before the scan was started.

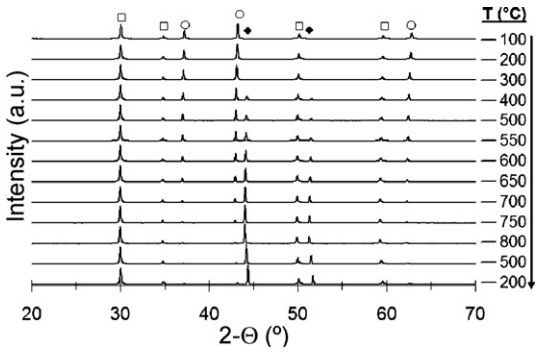

Fig. 1. *In situ* reduction (5% H_2/N_2) of NiO-YSZ monitored by XRD. Phases denoted as YSZ (□), NiO (◯), and Ni (♦). The arrow indicates chronological order.

3. Results

3.1. Activation of NiO-YSZ

Reduction of NiO to Ni in the as-received catalyst was studied by *in situ* XRD as shown in Fig. 1. The YSZ phase was stable in the temperature range studied. NiO (ICDD # 47–1049) began reducing around 500 °C and the reduction was completed near 700 °C. The disappearance of NiO coincided precisely with the appearance of metallic Ni (ICDD # 4–850). The intensity of the metallic Ni lines did not grow further above 700 °C. Therefore, a reduction at 700 °C for 1 h was selected as an appropriate reduction condition for the activation of the metallic Ni in the NiO-YSZ catalyst.

3.2. Influence of H_2S upon catalytic activity

The role of H_2S upon the catalytic activity was examined for selected anode chamber reactions. An outline of potential anode chamber reactions (limited to those involving only C, O, and H) is shown in Scheme 1. S-catalyst interactions were isolated by exposing the catalysts to various flows containing H_2S prior to fixed bed reactions. Since no active gases were present except H_2S during the hold at 700 °C, removal of S from the sample and structural changes caused during temperature ramps (e.g., phase changes occur under cooling when Ni-YSZ is exposed to streams containing H_2S [54]) were assumed negligible. This assumption was confirmed through isolated experiments under inert and oxidizing conditions, which also showed that S species (as SO_x) evolved only above 700 °C. Moreover, S species were not observed in the effluent under any of the reaction conditions. The effect of temperature was not examined in the present study as temperatures near 700 °C are expected to be used in efforts to balance advantages of higher and lower operation temperatures [1,23]. While these results suggested stable S species, it is possible that the bonding environment of S changes in different environments.

3.2.1. Effect of 50 ppm H_2S/N_2 upon activity for selected reactions over Ni-YSZ

Since CO is more difficult to electrochemically oxidize than H_2 for Ni-YSZ [55,56], stoichiometric CO oxidation was ini-

$$H_2 + O_x \xrightarrow{H_2\text{-oxidation}} H_2O$$

$$CO + O_x \xrightarrow{CO\text{-oxidation}} CO_2$$

$$CO + H_2O \underset{r\text{-}WGS}{\overset{WGS}{\rightleftharpoons}} CO_2 + H_2$$

$$CH_4 + 4O_x \xrightarrow{CH_4\text{-oxidation}} 2H_2O + CO_2$$

$$CH_4 + 2H_2O \underset{methanation}{\overset{steam\text{-}reforming}{\rightleftharpoons}} CO_2 + 4H_2$$

$$CH_4 + H_2O \underset{methanation}{\overset{steam\text{-}reforming}{\rightleftharpoons}} CO + 3H_2$$

$$CH_4 + CO_2 \underset{methanation}{\overset{dry\text{-}reforming}{\rightleftharpoons}} 2CO + 2H_2$$

$$2CO \xrightarrow{Boudouard} CO_2 + C$$

$$CO + H_2 \xrightarrow{CO\text{-}reduction} C + H_2O$$

$$CH_4 \xrightarrow{HC\text{-}decomposition} C + 2H_2$$

Scheme 1. Potential reactions in anode chamber when syngas used as fuel.

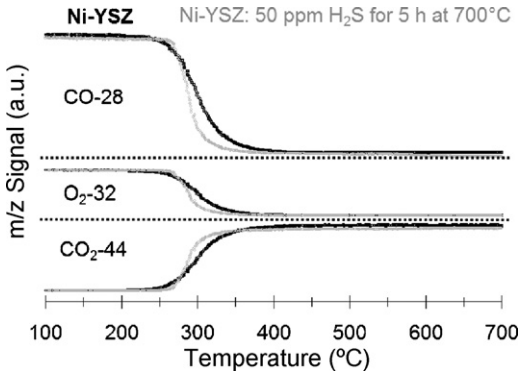

Fig. 2. Temperature-programmed reaction profiles for CO oxidation over Ni-YSZ with and without H_2S exposure prior to the reaction.

tially selected as a probe reaction. As shown in Fig. 2, exposure to 50 ppm H_2S/N_2 prior to the reaction did not influence activity. Quantified results for this reaction, as well as all others in this section, are summarized in Table 2. Moreover, deactivation was not observed during the 4 h on stream at 700 °C (data not shown) for either case. Additionally, a sequentially performed TPO did not show any evidence of coking. Since H_2S exposure did not influence the reaction, CO oxidation was a poor model reaction for examining the effect of S. This reaction may be affected minimally by H_2S exposure because the mechanism is different when involving gas-phase oxygen rather than electrochemical oxygen at the anode–electrolyte interface or because YSZ is able to turnover CO under similar conditions. CO oxidation over YSZ showed onset and light-off temperatures only slightly higher than those for Ni-YSZ (data not shown).

Consequently, the effect of S was further studied by analyzing isolated fuel processing reactions that influence the composition of C and H-containing gases in the anode chamber. These reac-

Table 2
Temperature-programmed reaction results for methane-steam reforming over Ni-YSZ with[a] and without H_2S exposure prior to the reaction

CO oxidation					
$T_{onset\text{-}CO}$ (°C)		$T_{50\text{-}CO}$ (°C)		C_{dep} (mg C/m^2/h)[b]	
No H_2S	50 ppm H_2S	No H_2S	50 ppm H_2S	No H_2S	50 ppm H_2S
263	260	308	295	n.d.	n.d.
Water-gas shift					
$T_{onset\text{-}CO}$ (°C)		Y_{H_2} at 700 °C (%)		C_{dep} (mg C/m^2/h)[b]	
No H_2S	50 ppm H_2S	No H_2S	No H_2S	No H_2S	50 ppm H_2S
300	479	69	28	n.d.	n.d.
Reverse water-gas shift					
$T_{onset\text{-}H_2}$ (°C)		Y_{H_2O} at 700 °C (%)		C_{dep} (mg C/m^2/h)[b]	
No H_2S	50 ppm H_2S	No H_2S	50 ppm H_2S	No H_2S	50 ppm H_2S
251	255	55	53	n.d.	n.d.
Methane-steam reforming					
$T_{onset\text{-}H_2}$ (°C)		Y_{H_2} at 700 °C (%)		C_{dep} (mg C/m^2/h)[b]	
No H_2S	50 ppm H_2S	No H_2S	50 ppm H_2S	No H_2S	50 ppm H_2S
314	351	45	<1	53	n.d.
Methane partial oxidation					
$T_{onset\text{-}H_2O}$ (°C)		Y_{H_2/CO_2} at 700 °C (%)		C_{dep} (mg C/m^2/h)[b]	
No H_2S	50 ppm H_2S	No H_2S	50 ppm H_2S	No H_2S	50 ppm H_2S
435	439	80/27	0/53	< 1	n.d.

[a] H_2S exposures at 700 °C for 5 h.
[b] n.d.: None detected.

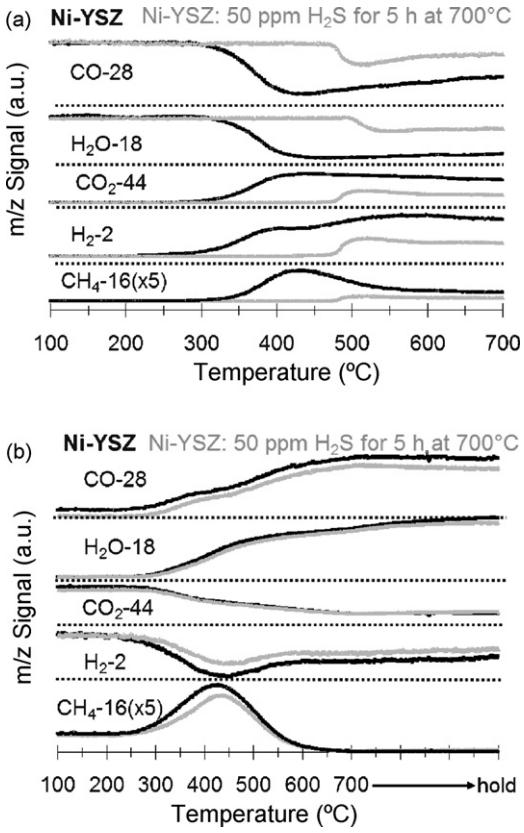

Fig. 3. Temperature-programmed reaction profiles for the (a) WGS and (b) r-WGS reactions over Ni-YSZ with and the without H_2S exposure prior to the reaction.

tions may occur near the anode–electrolyte interface, but also occur elsewhere, especially if the anode chamber is packed with Ni-YSZ to catalyze H_2 enrichment. The water-gas shift (WGS) and r-WGS reactions are common examples and these reactions do not reach equilibrium at SOFC operating temperatures since Ni is not as active as Cu- or Fe-based catalysts [57]. As presented in Fig. 3(a), WGS activity began near 300 °C. Once H_2 formed, a competing reaction, methanation, also occurred. Thermodynamic tendency to form CH_4 at intermediate temperatures is a factor in forcing SOFCs to operate at high temperatures [22]. After CH_4 formation decreased, extent of the WGS reaction declined as the reaction was thermodynamically limited (e.g., [58]). No further decline in the reaction was observed during the 4 h hold at 700 °C. After the catalyst was exposed to 50 ppm H_2S/N_2, initial activity was suppressed by almost 200 °C. Due to this temperature shift, methanation was also less prevalent. Since the CH_4 signal was weaker even after H_2 formed compared to the reaction when S was not introduced, S may also directly deactivate CH_4 formation (not just from a lack of H_2). The r-WGS reaction was also inspected and the results are presented in Fig. 3(b). While temperature increased, exposure to H_2S led to discernable differences only in the H_2 and CH_4 signals. These differences showed that sulfur affected the CH_4 formation, but not the r-WGS activity. Moreover, no carbon deposition was observed for any of the WGS or r-WGS reactions after 4 h of steady reaction at 700 °C. Analysis of the WGS and r-WGS reactions demonstrated that S impacted CH_4 formation. An important question that these experiments raised was why the WGS reaction is greatly impacted by S whereas the r-WGS is not. As discussed further in Section 4.2, the activation of H_2O likely occurred on a different site than the other species so the key difference between these two reactions is that water is a reactant in one and a product in the other.

Since CH_4 was produced under certain conditions and syngas contains appreciable levels of hydrocarbons, reactions involving CH_4 were also examined (Fig. 4). For CH_4–H_2O reforming (Fig. 4(a)), the temperature at which reforming began aligned well with the temperatures where methanation occurred during the WGS and r-WGS reactions. Unlike previously reported CH_4–H_2O reforming results over Ni-YSZ [59], deactivation was not observed during the 4 h on stream at 700 °C in this study. This difference was likely caused by differences in experimental conditions. For example, the steam-to-carbon ratio and temperatures were different and both can influence the degree of coke formation. Although no noticeable decline in CH_4 conversion or H_2 production was observed, a subsequent TPO experiment showed significant quantities of CO_2 formation, signaling carbon deposition on the surface (Fig. 4b). For the H_2S treated catalyst, the reaction behavior was similar at low temperatures (<525 °C), but very different at high temperatures (>525 °C). At lower temperatures, the H_2 yield was slightly lower over the S-treated sample, but the take-off temperature and the slope of the yield increase were quite comparable to what was observed over the S-free sample. Hence, although there appeared to be some loss of activity for the CH_4–H_2O reforming due to H_2S treatment, the effect was relatively small. At higher temperatures, however, the behavior was very different. Extent of reaction progressed through a maximum near 525 °C and, at higher temperatures, H_2 production as well as CH_4 and H_2O conversions declined. When a subsequent TPO experiment (Fig. 4b) was performed over the H_2S treated catalyst, no carbon deposition was observed. Differences between the S-free and S-treated catalysts in terms of the coke deposition and CH_4 conversion suggested that the reaction can be broken down into two regimes based on temperature. Below 525 °C, CH_4 conversion occurred through steam reforming and the H_2S treatment only showed a slight impact on activity. The primary reaction above 525 °C over the S-free catalyst was CH_4 decomposition. This reaction was inhibited by the H_2S treatment, which accounted for the lack of carbon deposition on the S-treated catalyst. This observation was consistent with previous reports in the literature where the introduction of small amounts of S contaminants was examined as a way to minimize coke formation during reforming [34–36,50,51]. However, this explanation cannot account for the nearly non-existent activity at 700 °C over the S-treated catalyst. Even if there were no CH_4 decomposition reaction over this catalyst because of S-treatment, it is difficult to explain why the steam reforming activity was not maintained. Because the present results do not offer a definitive answer to this question, CH_4–H_2O reforming is further examined as a function of H_2S exposure in Section 3.2.3 and possible explanations are discussed in Section 4.2.

As presented in Fig. 4(c), the role of sulfur was further examined through the CH_4 partial oxidation reaction. Over both S-treated and S-free catalysts, CH_4 conversion began near

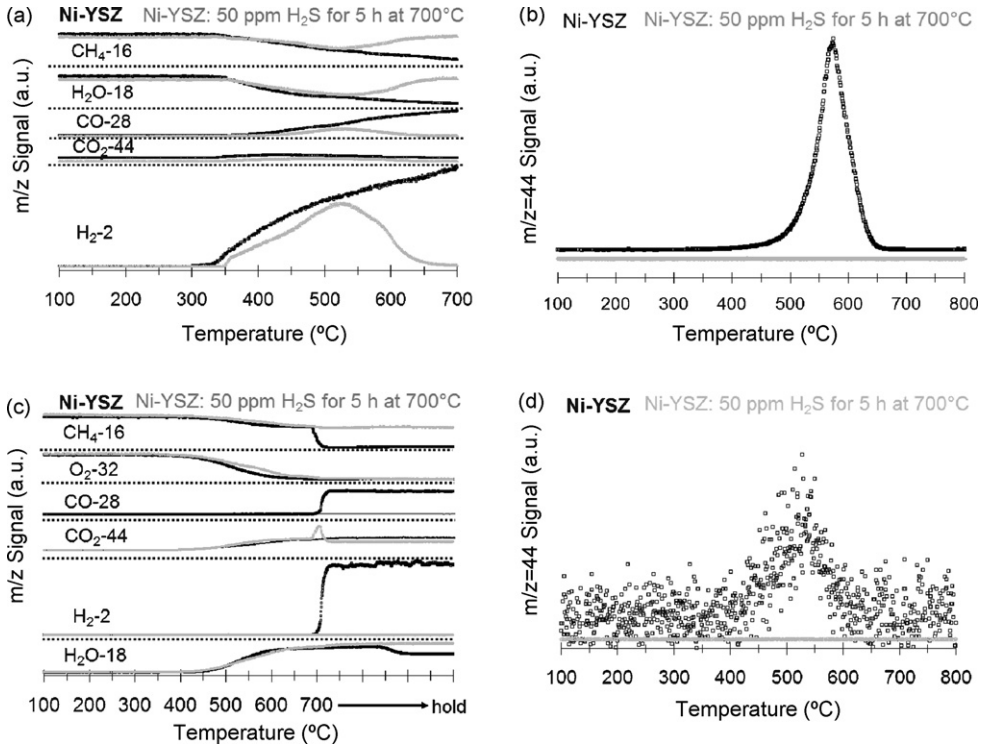

Fig. 4. Temperature-programmed reaction profiles for (a) methane-steam reforming with (b) coke oxidation during a sequential TPO and (c) partial methane oxidation with (d) coke oxidation during a sequential TPO over Ni-YSZ with and without H_2S exposure prior to the reaction.

400 °C, leading primarily to complete combustion of CH_4 to CO_2 and H_2O. This reaction progresses in a similar fashion over both catalysts until all of the O_2 was depleted, demonstrating that CH_4 combustion (similar to CO oxidation results) is not affected by the H_2S treatment. At this point, the CH_4 conversion is around 50%, the expected level based on the 1:1 CH_4/O_2 ratio used in the experiment. As the reaction continues at 700 °C, product distribution and CH_4 conversion show very different trends over the two catalysts. The S-free catalyst showed a sharp decrease in CH_4 concentration (i.e., increase in conversion) accompanied by a sharp increase in H_2 production and CO production. Increases in CH_4 conversion and H_2 production were likely caused by the hydrocarbon decomposition reaction, while CO formation could be due to partial oxidation of the coke. Over the S-treated sample, CH_4 conversion stayed at 50% and no H_2 was produced, indicating that the CH_4 decomposition reaction did not take place. Subsequent TPO experiments showed no coke deposition on the S-treated sample although significant coke formation existed on the S-free catalyst, supporting our earlier assertion that coke deposition was suppressed following H_2S treatment. Since O_2 is a better oxidant than H_2O, less coke formed during partial oxidation than during H_2O reforming.

3.2.2. *Effect of H_2S on the activity of YSZ for selected reactions*

Results for WGS reaction, CH_4–H_2O reforming and partial CH_4 oxidation over YSZ are summarized in Table 3. These reactions were repeated over YSZ alone to examine the impact

Table 3
Temperature-programmed reaction results for various reactions over YSZ with and without H_2S exposure prior to the reaction[a]

Water-gas shift					
$T_{onset\text{-}H_2}$ (°C)		C_{CO} at 700 °C (%)		Y_{H_2} at 700 °C (%)	
No H_2S	50 ppm H_2S	No H_2S	50 ppm H_2S	No H_2S	50 ppm H_2S
496	509	6	5	12	8
Methane-steam reforming					
$T_{onset\text{-}H_2}$ (°C)		C_{CH_4} at 700 °C (%)		Y_{H_2} at 700 °C (%)	
No H_2S	No H_2S	No H_2S	50 ppm H_2S	No H_2S	50 ppm H_2S
498	501	<1	<1	<1	<1
Methane partial oxidation					
$T_{onset\text{-}H_2O}$ (°C)		C_{CH_4} at 700 °C (%)		Y_{H_2/CO_2} at 700 °C (%)	
No H_2S	50 ppm H_2S	No H_2S	50 ppm H_2S	No H_2S	50 ppm H_2S
576	583	23	21	8/9	7/6

[a] H_2S exposures at 700 °C for 5 h.

of H_2S for the reactions which showed the largest differences over Ni-YSZ. Although activity was much lower without the Ni, reactions showed enough activity for a comparison. These reactions showed little influence of S deactivation as all measured parameters were in close proximity to each other. A slight shift to higher onset temperatures, lower reactant conversions, and lower product yields occurred following the H_2S exposure. Since the differences were small and the reactions showed no significant behavioral changes as Ni-YSZ did, the lower activity was attributed to physical differences caused by processing. YSZ was initially calcined in air at 550 °C for 3 h. Following this treatment, it was used in the reactions or further treated with H_2S at 700 °C for 5 h. Small performance differences likely originated from a loss of surface area during this additional treatment. Under oxidizing treatments, *in situ* XRD patterns of YSZ alone (data not shown) showed narrowing of its diffraction lines at temperatures in this range. Narrowing of the diffraction lines indicated an increase in crystallite size which would cause a decrease in total surface area.

3.2.3. Further examination of CH_4–H_2O reforming over Ni-YSZ

Since CH_4–H_2O reforming was highly influenced by S, reaction parameters, including the effects of H_2S exposure conditions, were examined in more depth (Table 4). Before examining H_2S exposure conditions in more detail, other parameters are discussed. When a lower ramp rate was used, the onset temperature shifted only 25 °C suggesting data taken during the temperature ramp were near steady-state levels and other values were similar indicating reproducibility. As the CH_4 to H_2O ratio in the feed increased, the reaction began at a similar temperature while the H_2 yield at 700 °C decreased. Moreover, the expected trend between C deposition and CH_4 to H_2O ratio was observed.

As illustrated in Section 3.2.1, the sample exposed to 50 ppm H_2S showed activity between 400 and 600 °C, but very little at 700 °C. The sample exposed to 500 ppm H_2S showed similar behavior but much lower activity (~1/10 of the maximum H_2 yield) than the 50 ppm H_2S sample. After Ni-YSZ was exposed to either 50 ppm H_2S for 24 h or 100 ppm H_2S for 5 h, no activity existed at any temperature. Following exposure to 50 ppm H_2S for 5 h, a sample was reduced (10% H_2/N_2 for 5 h) to examine if the catalyst could be regenerated to its pre-H_2S level by H_2 treatment. Other studies demonstrated a return of activity during operation under mixtures of H_2 and H_2O after H_2S deactivation [42,43]. Our results showed that this treatment actually led to decreased activity. While possible reasons are provided (it is possibly related to the lack of high-temperature CH_4–H_2O reforming activity after H_2S exposure) in Section 4.2, its negative influence inferred that H_2O was likely the source of regeneration in the aforementioned studies.

In all cases following the introduction of H_2S, no C deposits were detected. The remaining sections of this work are aimed at linking these differences in activity to bulk (Section 3.3) and surface (Section 3.4) characteristics induced by H_2S exposure.

3.3. Bulk characterization of Ni–S interactions

XRD patterns are shown in Fig. 5. As discussed in Section 3.1, YSZ was stable during the reduction of NiO and also remained stable during all H_2S treatments. Following all H_2S treatments, the only detectable phases were Ni and YSZ, which suggested that a bulk phase transition to a sulfide did not occur. Comparison to the diffraction pattern for Ni_3S_2 showed no indication of such a phase.

A similar analysis as to XRD was performed by laser Raman spectroscopy with the results presented in Fig. 6. The band near 624 cm^{-1} was attributed to a lattice vibration for YSZ [54,60]. Spectra for the three samples without H_2S exposure appeared similar with only this band present. For the H_2S exposed samples, an additional band appeared near 153 cm^{-1} in several

Table 4
Temperature-programmed reaction results for methane-steam reforming over Ni-YSZ with and without H_2S exposure prior to the reaction

Parameter altered	$T_{onset\text{-}H_2}$ (°C)	Y_{H_2} at 700 °C (%)	C_{dep}[a] (mg C/m^2/h)	S_C[a] (%)
Baseline[b]				
Ni-YSZ	314	45	53	32
Effect of ramp rate				
2 °C/min	339	51	49	30
Effect of CH_4:H_2O				
$CH_4/H_2O = 2.0$	314	33	61	45
$CH_4/H_2O = 0.5$	347	45	40	21
Effect of H_2S conc.				
50 ppm	351	<1	n.d.	n.d.
100 ppm	n.d.	n.d.	n.d.	n.d.
500 ppm	493	<1	n.d.	n.d.
Effect of H_2S time (h)				
50 ppm/24	n.d.	n.d.	n.d.	n.d.
Effect of post-reduction				
50 ppm/red	590	2	n.d.	n.d.

[a] n.d.: None detected.
[b] Baseline parameters: ramp rate = 10 °C/min, flow rate = 50 mL/min, $CH_4/H_2O = 1.0$, and no sulfur exposure.

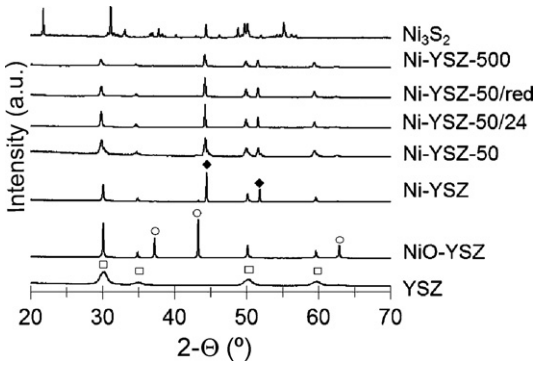

Fig. 5. XRD patterns at various stages of processing for NiO-YSZ. See Table 1 for notation. YSZ and Ni_3S_2 were provided as reference materials. Phases denoted as YSZ (□), NiO (◯), and Ni (♦).

of the samples. While this band was likely an indicator of a S-containing species, it occurred at a lower position than is normally reported. This band was not present in the sample that was reduced following H_2S exposure indicating a structural change. Additionally, a weak band near 350 cm^{-1} was observed for the samples exposed to 50 ppm H_2S for 24 h and 100 ppm H_2S for 5 h. This band may be caused by Ni_3S_2. It was no longer present in the samples exposed to 500 ppm H_2S for 5 h. However, a band, which could be caused by β-NiS [54], appeared near 250 cm^{-1}. Since the band at 153 cm^{-1} was not identified and the other bands were weak, definitive identification of the phases was not possible.

3.4. Surface characterization of Ni–S interactions

The lack of conclusive evidence for bulk species suggests that surface S led to the activity losses rather than bulk sulfur species. Surface spectra via XPS for various processing stages of Ni-YSZ catalysts are shown in Fig. 7. Based on these results and spectra for Y3d and Zr3d, surface compositions were calculated and are presented in Table 5. Binding energies for $Zr3d_{5/2}$ and $Y3d_{5/2}$ were near 181.6 and 156.4 eV, respectively. Both values were close to those of bulk metal oxides [61]. The composition ratio of Zr to Y was in the proper range as in the bulk with a slight preference for Y at the surface. A series of O1s peaks were

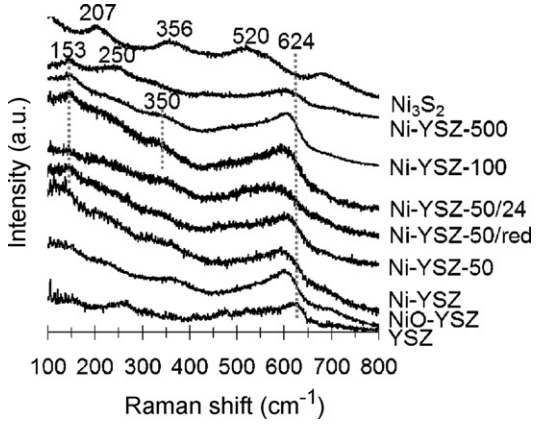

Fig. 6. Laser Raman spectra at various stages of processing for NiO-YSZ. See Table 1 for notation. YSZ and Ni_3S_2 were provided as reference materials.

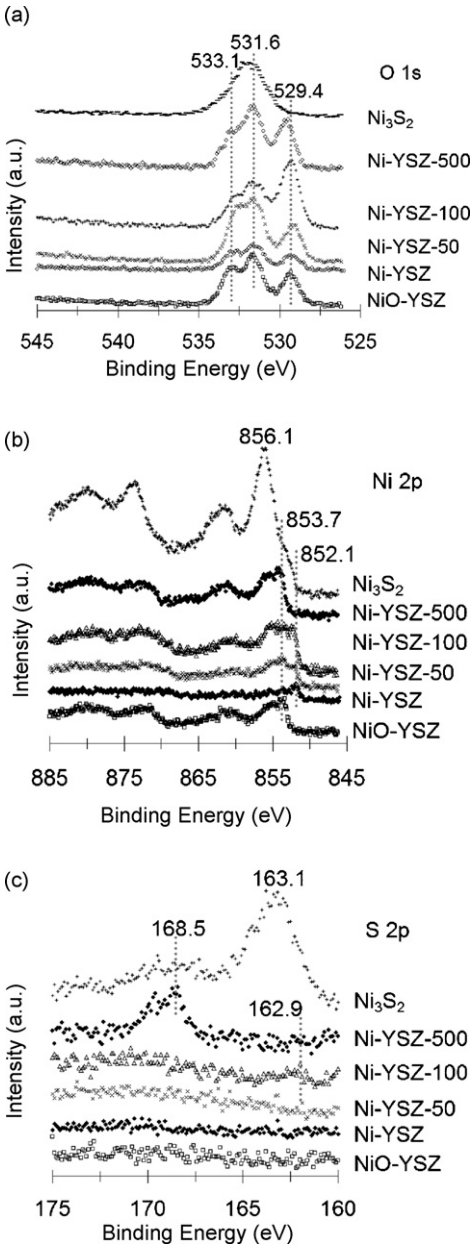

Fig. 7. Surface spectra by XPS for the (a) O1s, (b) Ni2p, and (c) S2p regions at various stages of processing for NiO-YSZ. See Table 1 for notation. Ni_3S_2 was provided as a reference material.

observed with binding energies near 529.4, 531.5, and 533.0 eV. The intermediate binding energy was attributed to O in YSZ. While O in ZrO_2 is expected near 531 eV [61], research also showed a shift towards higher values when Y is incorporated [62]. The lower peak was caused by either O in NiO [61] or pure Y_2O_3 [63]. Since there was a preference for Y at the surface over Zr and the peak was present for Ni-YSZ (when the Ni regions show NiO was not present), the latter was deemed more likely. The high binding energy peak was associated to adsorbed O species or impurities such as Si which can segregate in grain boundaries of YSZ.

Initially, peaks for $Ni2p_{3/2}$ were observed at binding energies of 854.1 and 856.1 eV indicating NiO and Ni in either a more

Table 5
Surface analyses from XPS shown in Fig. 7

Treatment	Region	BE (eV)	Composition (at %)
NiO-YSZ	$Ni2p_{3/2}$	854.1	9.5
	$Ni2p_{3/2}$	856.1	3.7
	O1s	529.4	22.3
	O1s	531.6	24.8
	O1s	533.1	18.1
	$Zr3d_{5/2}$	181.6	18.8
	$Y3d_{5/2}$	156.6	2.8
Ni-YSZ	$Ni2p_{3/2}$	852.2	7.4
	$Ni2p_{3/2}$	855.1	3.7
	O1s	529.3	16.0
	O1s	531.5	28.0
	O1s	532.9	17.8
	$Zr3d_{5/2}$	181.5	24.0
	$Y3d_{5/2}$	156.4	3.6
Ni-YSZ-50	$Ni2p_{3/2}$	852.7	4.6
	$Ni2p_{3/2}$	854.9	5.0
	O1s	529.2	15.4
	O1s	531.5	30.1
	O1s	532.8	16.2
	$Zr3d_{5/2}$	181.5	25.5
	$Y3d_{5/2}$	156.4	3.2
	$S2p_{3/2}$	–	–
Ni-YSZ-100	$Ni2p_{3/2}$	852.8	9.2
	$Ni2p_{3/2}$	855.3	6.3
	O1s	529.4	20.9
	O1s	531.4	16.5
	O1s	532.8	8.8
	$Zr3d_{5/2}$	181.6	33.4
	$Y3d_{5/2}$	156.6	4.9
	$S2p_{3/2}$	162.2	<0.1
Ni-YSZ-500	$Ni2p_{3/2}$	854.2	8.0
	$Ni2p_{3/2}$	856.3	7.6
	O1s	529.7	18.0
	O1s	531.6	24.1
	O1s	532.9	13.6
	$Zr3d_{5/2}$	181.8	23.4
	$Y3d_{5/2}$	156.8	4.9
	$S2p_{3/2}$	168.7	1.9
Ni_3S_2	$Ni2p_{3/2}$	856.0	88.2
	$S2p_{3/2}$	163.2	9.2
	$S2p_{3/2}$	168.0	2.6

oxidized form or organic species, respectively [61]. The presence of the satellite peak near 860 eV confirmed the presence of divalent species. Following reduction, the satellite peak shrunk and peaks shifted to lower binding energies showing the presence of metallic Ni [61] by the main peak at 852.2 eV. With H_2S exposure, peaks shifted back towards higher binding energies indicating interactions with S. For the 50 and 100 ppm exposed samples, binding energies near 853 eV indicated the presence of NiS [61]. Moreover, the satellite peak re-appeared confirming oxidation of Ni to a divalent species. The cause of the binding energy near 855 eV was not clear. It could be linked to the species originally at 856.1 eV. In the 500 ppm exposed sample, a pair of peaks was observed. The one with higher binding energy aligned with the major peak in the Ni_3S_2 standard, but could also be caused by an organic species. As discussed in analysis of the S2p region, the lower binding energy peak was likely caused by sulfate species.

S was not detectable easily in any of the samples with the exception of the 500 ppm exposed sample. For this treatment, the binding energy of 168.5 eV for $S2p_{3/2}$ was in the region for sulfate groups [61], which may be linked to the $Ni2p_{3/2}$ peak at 854.2 eV. A very small peak at 162.9 eV for the sample exposed to 100 ppm suggested a NiS phase [61] may be present at the surface in this sample. By comparison to the Ni_3S_2 standard, it was not possible to assign any of the XPS features to this species.

The effect of S on the surface of Ni-YSZ was also examined using CO as a probe molecule during *in situ* DRIFTS studies. In Fig. 8(a), DRIFT spectra are presented during a TPD following CO adsorption on the fresh Ni-YSZ surface. The only band observed was at 2042 cm^{-1} and was attributed to linearly adsorbed CO on metallic surface sites with low levels of interactions with the support [64–66]. The species was mostly desorbed by 500 °C. When CO was adsorbed after Ni-YSZ was treated

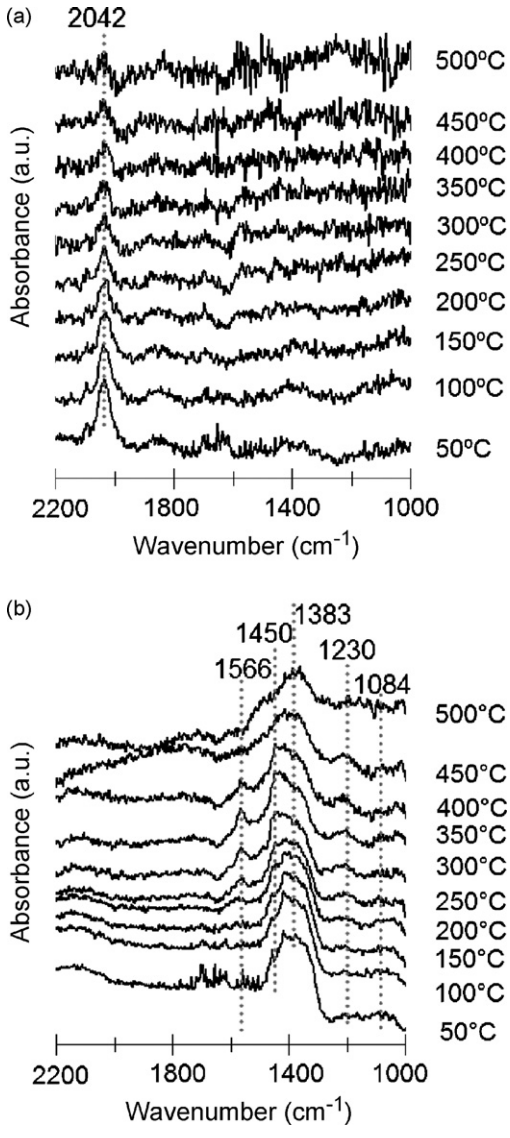

Fig. 8. *In situ* DRIFTS CO TPD over Ni-YSZ (a) without and (b) with exposure to 50 ppm H_2S/N_2 at 700 °C for 5 h prior to CO adsorption.

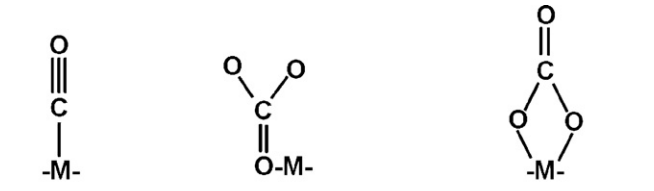

Scheme 2. Surface species observed in Fig. 8.

in 50 ppm H_2S at 700 °C for 5 h as shown in Fig. 8(b), bands were observed at 1566, 1450, 1383, 1230 and 1084 cm^{-1}. These bands indicated bidentate and monodentate carbonate species over Ni [64]. These species are compared to linearly bound CO in Scheme 2. While shifts of relative intensities existed with temperature (i.e., bands at 1230 and 1450 cm^{-1} grow stronger at 350 and 450 °C indicating greater stability of bidentate carbonates), the species were stable up to 500 °C, in contrast to the linearly bound CO observed over S-free sample. Despite some noise in the region, a small band near 1700 cm^{-1} at 50 °C may signify a small amount of bridged CO surface species [65].

4. Discussion

4.1. Trends between CH_4–H_2O reforming activity and characterization results

For CH_4–H_2O reforming, no activity existed after 50 ppm H_2S for 24 h or 100 ppm H_2S for 5 h. Both of these samples showed a weak band in Raman spectroscopy for Ni_3S_2. Since this phase was not observed in XRD or XPS and was only weakly observed by Raman spectroscopy, the results suggested Ni_3S_2 was enriched in micro-domains. Thus, incorporation of Ni into this phase appeared to be linked to the elimination of activity. Despite being exposed to a higher concentration of H_2S, the Ni-YSZ exposed to 500 ppm H_2S showed measurable, albeit low activity. The presence of activity coincided with indications that β-NiS (LRS) and/or surface sulfate species (XPS), which suggested that these S species may demonstrate higher reforming activity than Ni_3S_2.

The sample exposed to 50 ppm showed considerably more activity than any of the other treatments, but also more complex behavior most likely because only a portion of the active sites were covered. Unlike the samples exposed to higher concentrations of H_2S, the 50 ppm H_2S-treated sample showed no indication of sulfur species in Raman spectroscopy. From XPS, the amount of surface S can only be estimated as less than 0.1%. A shift in the binding energy of the $Ni2p_{3/2}$ indicated the presence of Ni–S interactions at the surface. This interaction was confirmed using DRIFTS as CO was no longer able to bond linearly after H_2S was introduced. The presence of different sites with and without H_2S exposure indicated preferential adsorption on metallic sites when not covered by S. When these sites are not available, CO is able to adsorb on other sites such as Ni–S moieties or the Ni-YSZ interface, but the intrinsic activity of these sites are much lower than that of Ni sites. These results implied that short-term exposure (~5 h but less than 24 h) to 50 ppm H_2S or less is tolerable, but extended time at this concentration or even shorter exposure to 100 ppm led to permanent deactivation potentially through a higher S-surface coverage and/or the formation of more stable sulfur species.

4.2. Influence of S over surface chemistry for Ni-YSZ

From the reaction network analysis performed in Section 3.2.1, exposure of Ni-YSZ to 50 ppm H_2S prior to reaction demonstrated the strongest influence over reactions involving CH_4 and/or H_2O as reactants. Since H_2O may be activated by YSZ and then spill over to Ni to oxidize C species, deleterious interactions between YSZ and S are possible explanations. However, reaction results in Section 3.2.2 over YSZ showed no evidence for deactivation through direct interactions between YSZ and S. Previously, such interactions were inferred [43] because SSZ showed better tolerance than YSZ [41]. More likely, the improved tolerance of Ni-SSZ over Ni-YSZ is contributed to either higher ionic mobility [1] or stability/morphology differences as the original authors explained [41]. The impact of S must then be attributed to Ni as was discussed in Section 4.1.

The presence of S inhibited coking by eliminating the CH_4 decomposition pathway, but also led to the loss of high-temperature activity. Without H_2S exposure, adsorbed C reacts with either adsorbed O or hydroxyl groups from dissociatively adsorbed H_2O or polymerizes to form a precursor to coke. The former reaction is limited kinetically by rate of H_2O adsorption and dissociation, which is why C deposition is a kinetic issue. The latter reaction (commonly referred to as the transition from C_α to C_β [35,36]) led to coke formation more rapidly since the dissolution of C into Ni facilitates the formation of C whiskers/fibers whereas the initial C species is more prone to gasification. There may be different explanations why the sulfur exposure may be preventing coke formation. First, S preferentially binds to the sites most active (surface steps) for coke formation and steam reforming activity [48,49]. With the most active sites for both reaction pathways blocked, C species can only react on the less active (terrace) sites. Although these sites are less active for gasification compared to the step sites, these sites are much less prone to form coke. That is, the less active site favored gasification over coke formation despite a decrease in activity. Secondly, adsorption of S onto Ni sites may be related to the amount of Ni atoms needed to form an active site. More Ni atoms are needed for coke formation than for gasification [48,49,51]. Adsorption of S onto Ni may prevent the participation of that Ni atom into an ensemble for which it is needed to form an active site for coke formation, but does not prevent gasification. Another possibility is the incorporation of the S into the Ni lattice, and inhibiting the dissolution of C into Ni, and hence suppressing coke formation. Incorporation of dopant elements into the Ni lattice was reported to prevent coking in hydrocarbon steam reforming over Ni/Al_2O_3 systems [67].

Blocking of Ni sites by sulfur can account for the lower performance, but it cannot explain all the reaction results. Deactivation was strong for CH_4–H_2O reforming and the WGS reaction whereas it was minimal or non-existent for the r-WGS

reaction, CO oxidation and CH_4 oxidation. From these results, a link between deactivation and H_2O as a reactant appeared. Since H_2O may be activated to form surface hydroxyl groups by the oxide component, interactions between YSZ and S may be the source of deactivation. Since YSZ was not directly poisoned by S, it is conceivable that S prevents activated H_2O species from reaching adsorbed C species on Ni. Possible scenarios include spillover to Ni sites or activation at the Ni-YSZ interface. Since the rate-limiting step for CH_4–H_2O reforming over Ni-YSZ is linked to the generation of H_2 from H_2O [37], deactivation in H_2O-containing reactions may indicate that S inhibits the mobility of activated H_2O species. DRIFTS results showed CO likely adsorbed on sites at the Ni-YSZ interface after exposure to H_2S and suggested that CH_4 and H_2O may be competing for the same interfacial sites after step sites are occupied by S.

The S-treated catalysts showed a loss of steam reforming activity at higher temperatures (although there was substantial activity at lower temperatures) and the loss of activity when S-treated catalysts were 'reduced' with H_2 indicated a change, caused by either temperature or H_2O exposure, in the surface sites. Migration of S to more active sites or reconstruction of the surface sites at certain temperatures and/or with H_2O exposure are possibilities. Reconstruction of surface Ni by S is supported by other studies which show that relevant reactions are structure sensitive over Ni (e.g., [36,47]). A S-induced increase in Ni surface density is believed to be a general phenomenon at elevated temperatures and high S-surface coverage [36]. Since steps are more active than terraces for CH_4 activation [48,49], a Ni surface density increase would cause a loss in activity. However, a more definitive interpretation of the observed results would require *in situ* and post-reaction characterization of S-exposed catalysts.

5. Conclusions

The effects of H_2S exposure conditions (H_2S concentration, exposure time, and post-exposure reduction) were studied for CH_4–H_2O reforming over Ni-YSZ. Reactions with H_2O (WGS, steam reforming) were more strongly impacted by H_2S compared to CO or CH_4 oxidation reactions. H_2S treatments were also shown to eliminate the hydrocarbon decomposition pathway at high temperatures during reactions involving CH_4. Changes in the steam reforming activity over S-treated samples with increasing temperature or with high-temperature H_2 treatment suggest a change in the active sites. S migration to more active sites or surface restructuring with temperature remain as possibilities. These changes appeared to be accelerated by the presence of H_2O. Examination of H_2S treatments upon the activity for various SOFC anode chamber fuel processing reactions over Ni-YSZ is important for the mechanistic understanding of the reaction network with C-based fuels containing H_2S.

Acknowledgments

The financial support provided for this work by the Ohio Coal Development Office and the Ohio Department of Development through a Wright Center of Innovation is gratefully acknowledged. The authors would also like to acknowledge NSF support for acquisition of the XPS system under NSF-DMR grant #0114098 and to thank NexTech Materials for supplying the NiO-YSZ.

References

[1] R.M. Ormerod, Chem. Soc. Rev. 32 (2003) 17.
[2] M.C. Williams, J.P. Strakey, W.A. Surdoval, L.C. Wilson, Solid State Ion. 177 (2006) 2039.
[3] M. Gong, X. Liu, J. Trembly, C. Johnson, J. Power Sources 168 (2007) 289.
[4] M. Liu, G. Wie, J. Luo, A.R. Sanger, K.T. Chuang, J. Electrochem. Soc. 150 (2003) A1025.
[5] Z. Xu, J. Luo, K.T. Chuang, J. Electrochem. Soc. 154 (2007) B523.
[6] J.W. Fergus, Solid State Ion. 177 (2006) 1529.
[7] S. Tao, J.T.S. Irvine, Chem. Record 4 (2004) 83.
[8] T. Ishihara, S. Fukui, M. Enoki, H. Matsumotoa, J. Electrochem. Soc. 153 (2006) A2085.
[9] L. Aguilar, S. Zha, Z. Cheng, J. Winnick, M. Liu, J. Power Sources 135 (2004) 17.
[10] Z. Cheng, S. Zha, L. Aguilar, D. Wang, J. Winnick, M. Liu, Electrochem. Solid-State Lett. 9 (2006) A31.
[11] S. Hui, A. Petric, J. Eur. Ceram. Soc. 22 (2002) 1673.
[12] O.A. Marina, N.L. Canfield, J.W. Stevenson, Solid State Ion. 149 (2002) 21.
[13] P.R. Slater, D.P. Fagg, J.T.S. Irvine, J. Mater. Chem. 7 (1997) 2495.
[14] B.D. Madsen, S.A. Barnett, Solid State Ion. 176 (2005) 2545.
[15] B.D. Madsen, S.A. Barnett, J. Electrochem. Soc. 154 (2007) B501.
[16] S. Tao, J.T.S. Irvine, J.A. Kilner, Adv. Mater. 17 (2005) 1734.
[17] S. Zha, P. Tsang, Z. Cheng, M. Liu, J. Solid State Chem. 178 (2005) 1844.
[18] Y.-H. Huang, R.I. Dass, Z.-L. Xing, J.B. Goodenough, Science 312 (2006) 254.
[19] Y.-H. Huang, R.I. Dass, J.C. Denyszyn, J.B. Goodenough, J. Electrochem. Soc. 153 (2006) A1266.
[20] G. Pudmich, B.A. Boukamp, M. Gonzalez-Cuenca, W. Jungen, W. Zipprich, F. Tietz, Solid State Ion. 135 (2000) 433.
[21] S. Hui, A. Petric, Solid State Ion. 143 (2001) 275.
[22] R.J. Gorte, AICHE J. 51 (2005) 2377.
[23] S. McIntosh, R.J. Gorte, Chem. Rev. 104 (2004) 4845.
[24] S. Park, J.M. Vohs, R.J. Gorte, Nature 404 (2000) 265.
[25] H. Kim, S. Park, J.M. vohs, R.J. Gorte, J. Electrochem. Soc. 148 (2001) A693.
[26] R.J. Gorte, H. Kim, J.M. Vohs, J. Power Sources 106 (2002) 10.
[27] H. Kim, C. Lu, W.L. Worrell, J.M. vohs, R.J. Gorte, J. Electrochem. Soc. 149 (2002) A247.
[28] H. He, R.J. Gorte, J.M. Vohs, Electrochem. Solid-State Lett. 8 (2005) A279.
[29] Y.M. Choi, C. Compson, M.C. Lin, M. Liu, Chem. Phys. Lett. 421 (2006) 179.
[30] M.D. Gross, J.M. Vohs, R.J. Gorte, J. Electrochem. Soc. 153 (2006) A1386.
[31] M. Itome, A.E. Nelson, Catal. Lett. 106 (2006) 21.
[32] E. Nikolla, A. Holewinski, J. Schwank, S. Linic, J. Am. Chem. Soc. Commun. 128 (2006) 11354.
[33] B. Huang, S.R. Wang, R.Z. Liu, T.L. Wen, J. Power Sources 167 (2007) 288.
[34] J.R. Rostrup-Nielsen, Catal. Today 37 (1997) 225.
[35] C.H. Bartholomew, Catal. Rev.-Sci. Eng. 24 (1982) 67.
[36] C.H. Bartholomew, Appl. Catal. A: Gen. 212 (2001) 17.
[37] Z. Yu, S.S.C. Chuang, Appl. Catal. A: Gen. 327 (2007) 147.
[38] J.R. Rostrup-Nielsen, J. Catal. 85 (1984) 31.
[39] J. Liu, S.A. Barnett, Solid State Ion. 158 (2003) 11.
[40] A. Weber, B. Sauer, A.C. Muller, D. Herbstritt, E. Ivers-Tiffee, Solid State Ion. 152–153 (2002) 543.
[41] K. Sasaki, K. Susuki, A. Iyoshi, M. Uchimura, N. Imamura, H. Kusaba, Y. Teraoka, H. Fuchino, K. Tsujimoto, Y. Uchida, N. Jingo, J. Electrochem. Soc. 153 (2006) A2023.
[42] Y. Matsuzaki, I. Yasuda, Solid State Ion. 132 (2000) 261.

[43] S. Zha, Z. Cheng, M. Liu, J. Electrochem. Soc. 154 (2007) B201.
[44] J.P. Trembly, A.I. Marquez, T.R. Ohrn, D.J. Bayless, J. Power Sources 158 (2006) 263.
[45] A.I. Marquez, T.R. Ohrn, J.P. Trembly, D.C. Ingram, D.J. Bayless, J. Power Sources 164 (2007) 659.
[46] J. Dong, Z. Cheng, S. Zha, M. Liu, J. Power Sources 156 (2006) 461.
[47] J. Hepola, J. McCarty, G. Krishnan, V. Wong, Appl. Catal. B: Environ. 20 (1999) 191.
[48] F. Abild-Pedersen, O. Lytken, J. Engbæk, G. Nielsen, I. Chorkendorff, J.K. Nørskov, Surf. Sci. 590 (2005) 127.
[49] H.S. Bengaard, J.K. Nørskov, J. Sehested, B.S. Clausen, L.P. Nielsen, A.M. Molenbroek, J.R. Rostrup-Nielsen, J. Catal. 209 (2002) 365.
[50] D.L. Trimm, Catal. Today 37 (1997) 233.
[51] J.R. Rostrup-Nielsen, J. Sehested, Adv. Catal. 47 (2002) 65.
[52] D.E. Resasco, B.K. Marcus, C.S. Huang, V.A. Durante, J. Catal. 146 (1994) 40.
[53] E.J. Erekson, C.H. Bartholomew, Appl. Catal. 5 (1983) 323.
[54] Z. Cheng, M. Liu, Solid State Ion. 178 (2007) 925.
[55] R.L. Zahradnik, J. Electrochem. Soc. 117 (1970) 1443.
[56] O. Costa-Nunes, R.J. Gorte, J.M. Vohs, J. Power Sources 141 (2005)241.
[57] K. Ahmed, K. Foger, J. Power Sources 103 (2001) 150.
[58] S. Natesakhawat, X. Wang, L. Zhang, U.S. Ozkan, J. Mol. Catal. A: Chem. 260 (2006) 82.
[59] N. Laosiripojana, S. Assabumrungrat, J. Power Sources 163 (2007) 943.
[60] M.B. Pomfret, J.C. Owrutsky, R.A. Walker, J. Phys. Chem. B Lett. 110 (2006) 17305.
[61] J.F. Moulder, W.F. Stickle, P.E. Sobol, K.D. Bomben, Handbook of X-Ray Photoelectron Spectroscopy, second ed., Perkin-Elmer Corporation, Eden Prairie, MN, 1992.
[62] I. Valov, R.A. De Souza, C.Z. Wang, A. Borger, C. Korte, M. Martin, K.-D. Becker, J. Janek, J. Mater. Sci. 42 (2007) 1931.
[63] M.B. Korzenski, Ph. Lecoeur, B. Mercey, D. Chippaux, B. Raveau, R. Desfeux, Chem. Mater. 12 (2000) 3139.
[64] S. Natesakhawat, O. Oktar, U.S. Ozkan, J. Mol. Catal. A: Chem. 241 (2005) 133.
[65] J. Ryczkowski, Catal. Today 68 (2001) 263.
[66] A. Diaz, L.M. Gandia, J.A. Odriozola, M. Montes, J. Catal. 162 (1996) 349.
[67] S. Natesakhawat, R.B. Watson, X. Wang, U.S. Ozkan, J. Catal. 234 (2005) 496.